Magn Reson Mater Phy (2015) 28:149–159
DOI 10.1007/s10334-014-0456-1

RESEARCH ARTICLE

K-t GRAPPA-accelerated 4D flow MRI of liver hemodynamics: influence of different acceleration factors on qualitative and quantitative assessment of blood flow

Zoran Stankovic · Jury Fink · Jeremy D. Collins · Edouard Semaan · Maximilian F. Russe · James C. Carr · Michael Markl · Mathias Langer · Bernd Jung

Received: 23 January 2014 / Revised: 8 July 2014 / Accepted: 18 July 2014 / Published online: 7 August 2014

Abstract
Objective We sought to evaluate the feasibility of k-t parallel imaging for accelerated 4D flow MRI in the hepatic vascular system by investigating the impact of different acceleration factors.
Materials and methods k-t GRAPPA accelerated 4D flow MRI of the liver vasculature was evaluated in 16 healthy volunteers at 3T with acceleration factors $R = 3$, $R = 5$, and $R = 8$ ($2.0 \times 2.5 \times 2.4$ mm^3, TR = 82 ms), and $R = 5$ (TR = 41 ms); GRAPPA $R = 2$ was used as the reference standard. Qualitative flow analysis included grading of 3D streamlines and time-resolved particle traces. Quantitative evaluation assessed velocities, net flow, and wall shear stress (WSS).
Results Significant scan time savings were realized for all acceleration factors compared to standard GRAPPA $R = 2$ (21–71 %) ($p < 0.001$). Quantification of velocities and net flow offered similar results between k-t GRAPPA $R = 3$ and $R = 5$ compared to standard GRAPPA $R = 2$. Significantly increased leakage artifacts and noise were seen between standard GRAPPA $R = 2$ and k-t GRAPPA $R = 8$ ($p < 0.001$) with significant underestimation of peak velocities and WSS of up to 31 % in the hepatic arterial system ($p < 0.05$). WSS was significantly underestimated up to 13 % in all vessels of the portal venous system for k-t GRAPPA $R = 5$, while significantly higher values were observed for the same acceleration with higher temporal resolution in two veins ($p < 0.05$).
Conclusion k-t acceleration of 4D flow MRI is feasible for liver hemodynamic assessment with acceleration factors $R = 3$ and $R = 5$ resulting in a scan time reduction of at least 40 % with similar quantitation of liver hemodynamics compared with GRAPPA $R = 2$.

Keywords 4D flow MRI · Liver hemodynamics · k-t GRAPPA · Quantification · Wall shear stress

Z. Stankovic (✉) · J. D. Collins · E. Semaan · J. C. Carr · M. Markl
Department of Radiology, Feinberg School of Medicine, Northwestern University, 737 N Michigan Avenue Suite 1600, Chicago, IL 60611, USA
e-mail: zoran.stankovic@northwestern.edu

Z. Stankovic · J. Fink · M. F. Russe · M. Langer
Department of Diagnostic Radiology and Medical Physics, University Medical Center Freiburg, Freiburg, Germany

M. Markl
Department of Biomedical Engineering, McCormick School of Engineering, Northwestern University, Chicago, IL, USA

B. Jung
Department of Radiology, University Hospital Bern, Bern, Switzerland

Introduction

Liver cirrhosis represents an important cause of morbidity and mortality in the United States [1]. Associated changes in the hepatic sinusoidal vascular resistance can result in portal hypertension. Portosystemic shunts spontaneously develop between the portal and systemic venous systems providing alternative drainage pathways. In addition to the elevated hepatic vascular resistance, patients develop a hyperdynamic syndrome with elevated portal blood flow, exacerbating the portosystemic pressure gradient increasing the cardiac output due to arteriovenous shunting [2]. Thus, it may be clinically relevant to measure hepatic blood flow parameters including peak velocity and net flow rate to evaluate changes in flow patterns in response to medical therapy [3, 4]. An additional parameter gaining interest in

cardiovascular diseases and preclinical studies is wall shear stress (WSS), which enables a better understanding of the influence of blood flow on the endothelium and risk for vascular remodeling (e.g. arteriosclerosis) [5–7].

Time-resolved (cine) phase contrast (PC) MRI (4D flow MRI) has been applied for the assessment of flow patterns in the heart [8], thoracic [9, 10] and abdominal aorta [11], and liver vasculature [12–16]. This technique enables a comprehensive evaluation of 3D flow patterns with full anatomic coverage and the ability for retrospective regional flow quantification [8–16]. One of the main limitations of 4D flow MRI is a lengthy total scan time of approximately 15–23 min [12, 14], limiting routine clinical use.

MRI is a standard clinical imaging technique for patients with advanced liver disease enabling morphologic and functional assessment of the liver with diffusion [17], perfusion [18], and elastography [19]. k-t GRAPPA accelerated 4D flow MRI is a non-contrast and reproducible technique which has the potential to impact clinical care meaningfully by acquiring metrics of peak velocities, net flow, and WSS in the hepatic system. Peak velocities and net flow represent established clinical metrics for portal hypertension while WSS represents an emerging parameter in preclinical studies [3–5, 7]. These changes may enable new therapeutic endpoints of medical therapy, assist in the evaluation of suspected vascular complications in liver transplantation, and quantify transjugular intrahepatic portosystemic shunt function [20]. However, the principle factor limiting broad clinical application of 4D flow MRI is the lengthy total scan time. In order to integrate this technique into the clinical workflow it is crucial to reduce the scan time. MR imaging for the broadly accepted clinical MRA of the heart reports single scan times between 7 and 10 min [21, 22]. k-t GRAPPA-accelerated 4D flow MRI can achieve similar scan times for liver flow analysis, opening a new window for a more thorough understanding of the complex changes in blood flow in the liver and portal venous system.

Fast sampling techniques like radial imaging with 3D PC VIPR (phase-contrast vastly under-sampled isotropic projection reconstruction) and improved respiratory gating or parallel imaging enables 4D flow scans in 8–20 min [23, 24]. Conventional acceleration techniques such as GRAPPA (Generalized Autocalibrating Partially Parallel Acquisitions) [25] or SENSE (sensitivity encoding) [26] typically enable scan time reduction by a factor of $R = 2$–3; higher values for R may adversely impact the quantification of velocities due to a lower signal to noise ratio [27]. Further developments of spatio-temporal parallel imaging techniques such as k-t principal component analysis (k-t PCA) [28], k-t GRAPPA [29], and k-t SENSE [30] allow higher acceleration factors and are promising techniques to reduce scan time for 4D flow MR imaging. However, temporal filtering may occur for higher acceleration factors thereby affecting the precision of the 4D flow data acquisition, flow visualization, and quantification [31]. A detailed assessment of different acceleration factors in k–t-based parallel imaging in the arterial and portal venous liver hemodynamics is lacking and necessary before clinical application of this acceleration technique to evaluate the hepatic vasculature.

The purpose of this study was, therefore, to evaluate systematically the impact of different acceleration factors in k-t GRAPPA-accelerated 4D flow MRI on scan times, image quality, and quantifiable hemodynamic biometric parameters.

Materials and methods

Study population

The study population consisted of 16 healthy volunteers without a history of clinical liver disease (10 women and 6 men, mean age = 24.5 ± 2.1 years). Written informed consent was received from all volunteers before MRI investigation. Study approval was obtained from our local institutional review board.

MR imaging

All measurements were performed at 3T (Magnetom Trio, Siemens Medical Systems, Erlangen, Germany). Data were acquired by a non-contrast enhanced 3D time-resolved rf-spoiled phase contrast gradient echo sequence, with three-directional velocity encoding (4D flow MRI) and a velocity encoding gradient (venc) of 100 cm/s [24]. This venc was chosen in order to evaluate the high flow within the arteries of the splanchnic system, while maintaining the ability to assess flow within the portal venous system. Respiratory gating at the lung–spleen interface was used to reduce image blurring and to minimize ghosting artifacts as described previously [24]. 4D flow MRI acquisition included prospective ECG-gating combining *k*-space segmented data acquisition with $N_k = 4$ phase encoding lines for each cardiac time frame. A six-element spine coil and a flexible six-element chest coil represented the receiver system. 4D flow data acquisition was performed in an axial oblique 3D volume oriented to the main portal vein with complete volumetric coverage of the hepatic arterial and portal venous vasculature.

Five 4D flow MRI datasets were acquired for each of the 16 volunteers during the same MRI examination. Participants were instructed to fast for 6 h prior to each scan to match liver physiology at the time of scanning. In the first step, a standard GRAPPA sequence was performed with

undersampling along the phase encoding (ky) direction with a reduction factor of $R = 2$. Afterwards, k–t-accelerated 4D flow MRI scans (i.e. undersampling along ky, kz, and t dimensions) were acquired with acceleration factors $R = 3$, $R = 5$, and $R = 8$ as described previously [32]. All of these scans were performed with a temporal resolution of about 82 ms. Additionally, one k-t GRAPPA scan with $R = 5$ was acquired with a temporal resolution of 41 ms (HR k-t GRAPPA 5 Tres41). The number of autocalibration (ACS) lines, resulting in a nominal acceleration R_{net} for the different acceleration factors R, as well as further pulse sequence parameters are provided in Table 1. The k-t algorithm was integrated into the scanner's data reconstruction workflow and all undersampled data were acquired and reconstructed directly on the MR system. For each acquisition, the total scan time was recorded. The following scan parameters were held constant across all 4D flow acquisitions: imaging matrix 160 × 100, FOV 200 × 320 mm^2, bandwidth 450 Hz/Pixel, venc 100 cm/s, and flip angle 7°.

Spatiotemporal data acquisition

Spatiotemporal (k-t) undersampling and reconstruction was applied using PEAK GRAPPA [32]. This technique represents an extension of k-t GRAPPA as described by Huang et al. [29]. PEAK GRAPPA is represented by a consistent reconstruction kernel geometry combining the smallest cell within a ky–kz–t data undersampling pattern. Data acquisition and reconstruction with different reduction factors ($R = 3$, $R = 5$, and $R = 8$) were applied using different sampling patterns and reconstruction kernels. A more detailed description of the sampling patterns and reconstruction kernels is provided in the work of Jung et al. [31].

Data analysis

Maxwell corrections to reduce phase offset errors were applied as described by Bernstein et al. [33] during the image reconstruction on the MR system. 4D flow MRI data were pre-processed using a home built analysis tool (programmed in Matlab, MathWorks, USA) that included noise filtering, velocity anti-aliasing [34], and correction for eddy currents, as previously described by Walker et al. [35]. Afterwards, a 3D PC MR angiogram (MRA) of the hepatic vascular system was calculated to create an iso-surface rendering of the vascular system (EnSight, CEI, Apex, USA) [36]. Based on the 3D PC MRA, ten analysis planes were manually placed in the measured 3D volume at the splenic and superior mesenteric veins, the splenic–mesenteric confluence, the intrahepatic main portal vein, the right and left intrahepatic portal vein branches, the celiac trunk, and the hepatic, splenic, and superior mesenteric arteries (Fig. 1).

3D blood flow visualization

The ten analysis planes represented emitter planes for the calculation of 3D streamlines (representing tri-directional blood flow velocities for individual cardiac time-frames) and time-resolved 3D particle traces (showing the temporal evolution of blood flow over the cardiac cycle) [37]. 3D display software was used to enable visual grading of the streamlines and particle traces from any view angle (EnLiten, CEI, Apex, USA). For each of the ten vessels, two independent, experienced readers blinded to acquisition type and subject identity quantitatively assessed image quality. Visibility of the above-described vessels based on the iso-surface rendering of the liver arterial and portal venous systems

Table 1 Summary of sequence parameters for standard GRAPPA $R = 2$ and four k-t GRAPPA-accelerated 4D flow MRI acquisitions with different acceleration factors applied in 16 healthy volunteers

	GRAPPA 2	k-t GRAPPA 3	k-t GRAPPA 5	k-t GRAPPA 5 Tres41	k-t GRAPPA 8
Reduction factor R	2	3	5	5	8
Spat. resolution (mm^3)	2.0 × 2.5 × 2.4	2.0 × 2.6 × 2.4	2.0 × 2.6 × 2.4	2.0 × 2.5 × 2.4	2.0 × 2.5 × 2.4
Temp. resolution (ms)	82	83	82	41	82
TE (ms)	2.6	2.8	2.6	2.6	2.6
ACS lines (ky × kz)	24 × Nz	18 × 6	20 × 7	20 × 7	16 × 7
R_{net}	1.6	2.8	4.2	4.2	6.3
Total scan time (min)	13.9 ± 3.6	8.2 ± 2.4*	8.1 ± 2.6*	11.0 ± 3.5*	4.0 ± 1.7*

Spat. spatial, *Temp.* temporal, *FOV* field of view, *venc* velocity encoding, *ACS* number of auto calibration lines, R_{net} resulting nominal acceleration

* Significant differences were present in scan times between standard GRAPPA $R = 2$ compared to k-t GRAPPA $R = 3$, $R = 5$ (temporal resolution 82 ms), $R = 5$ (temporal resolution 41 ms), and $R = 8$ ($p < 0.001$)

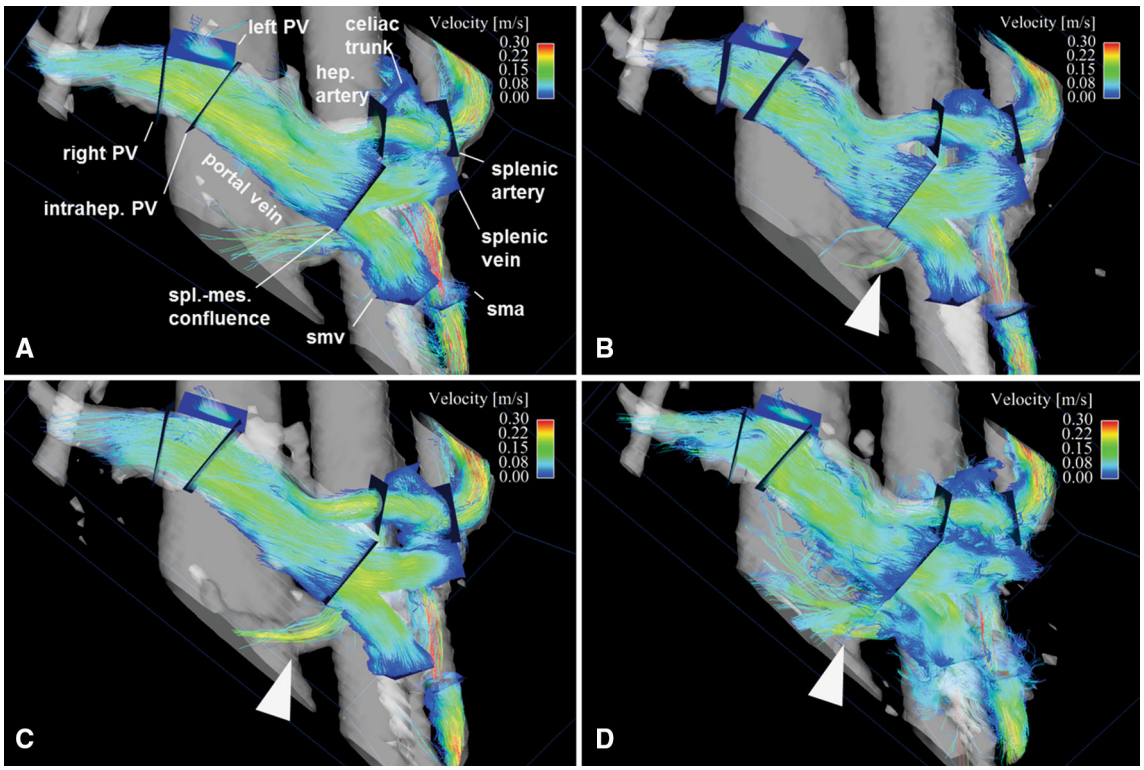

Fig. 1 3D particle traces visualization of the hepatic arterial and portal venous system with ten analysis planes for standard GRAPPA $R = 2$ (**a**) and acceleration factors k-t GRAPPA $R = 3$ (**b**), $R = 5$ (**c**), and $R = 8$ (**d**). The *blue* 2D analysis planes were manually positioned in the splenic vein, superior mesenteric vein (smv), splenic–mesenteric confluence (spl.-mes. confluence), intrahepatic portal vein (intrahep. PV), *right* (right PV) and *left* (left PV) intrahepatic portal vein branches, celiac trunk, splenic artery, hepatic artery (hep. artery), and superior mesenteric artery (sma). Increased leakage artifacts into neighboring vessels can be appreciated with higher acceleration factor, especially for k-t GRAPPA $R = 8$ compared to the standard GRAPPA $R = 2$ (*white arrowhead*). Color coding = local blood flow velocity

was graded on a three-point Likert scale (0 = not visible, 1 = partially visible, 2 = completely visible) [38]. Particle trace leakage artifacts, defined as 3D traces leaving the vessel lumen into adjacent vessels due to partial volume effects, were reported as present or not present (Fig. 1; Table 2).

Pathline visualization was independently evaluated by the same two observers blinded to scan type on a three-point Likert scale based on particle traces emitted from the splenic–mesenteric confluence (0 = particle traces reach only the intrahepatic portal vein, 1 = particle traces reach proximal part of the intrahepatic portal vein branches, 2 = particle traces reach the distal part of the intrahepatic portal vein branches). Furthermore, a quality grading of the 3D visualization by examining the temporal evolution of particle traces over the cardiac cycle was performed.

For each of the different k-t GRAPPA acquisitions, noise within the 3D volume was quantitatively evaluated by the same two independent, experienced readers blinded to acquisition type and subject identity based on a three-point scale (0 = no noise visible, 1 = occasional noise visible, 2 = distinct noise visible).

Table 2 Summary of 3D flow visualization (grade 2 for complete visibility) in 16 volunteers for $n = 80$ 4D flow data sets by readers A and B

	Visibility	
	Reader A	Reader B
Superior mesenteric vein	100 %	100 %
Splenic vein	100 %	100 %
Splenic–mesenteric confl.	100 %	100 %
Portal vein right branch	94 %	94 %
Portal vein left branch	53 %	51 %
Celiac trunk	100 %	100 %
Hepatic artery	100 %	100 %
Splenic artery	100 %	100 %
Superior mesenteric artery	100 %	100 %
Particle traces leakage	Present in 63 %	Present in 59 %

3D blood flow quantification

Blood flow quantification for all ten analysis planes within the arterial (four vessels) and portal venous (six vessels)

system was based on a home-built tool (programmed in Matlab, Mathworks, USA). Vessel lumen contours were manually delineated for each of the above mentioned vessel segments at each cardiac time frame. The segmentation was performed on standard GRAPPA 2 datasets and applied to the other four 4D flow MRI scans with k-t GRAPPA $R = 3$, $R = 5$, $R = 8$ and k-t GRAPPA 5 Tres41. When necessary the segmentation masks were adapted to the vessel lumen contour. Maximum and mean volumetric systolic velocities, net flow volume over the cardiac cycle and average wall shear stress (WSS) magnitude were calculated for each vessel segment [39].

Statistical analysis

Statistical analysis was performed using commercially available software (SPSS 19.0; SPSS, Chicago, IL, USA). Continuous variables were presented as mean ± standard deviation. Inter-observer agreement was evaluated using Cohen's kappa statistics. Kappa values were interpreted as follows: 0.21–0.40 fair agreement, 0.41–0.60 moderate agreement, 0.61–0.80 substantial agreement, and 0.81–1.00 excellent agreement, as described previously [40].

k-t-accelerated scans were compared to standard GRAPPA $R = 2$ by evaluating continuous variables using paired, two tailed t tests. A p value <0.05 was considered statistically significant. Different k-t GRAPPA acquisitions for all volunteers and analysis planes were compared to the standard GRAPPA $R = 2$ acquisition by the Bland–Altman approach using the mean difference (d) and standard deviation of the difference (s), calculating the limits of agreement (±2 SD) using 95 % confidence intervals [41].

Results

4D flow MRI scans using standard GRAPPA $R = 2$ and all four different acceleration factors were acquired and reconstructed in all subjects. A total of $n = 80$ hepatic 4D flow MRI data sets were analysed. Across the study cohort the average heart rate was 60.6 ± 9.2 bpm without significant variability between the different 4D flow MRI scans.

k-t GRAPPA acceleration factors of $R = 3$ and higher resulted in a significantly shorter average total acquisition time compared to standard GRAPPA $R = 2$ ($p < 0.001$) (Table 1). k-t GRAPPA $R = 3$ and $R = 5$ resulted in an average scan time reduction of 41 and 42 %, respectively. k-t GRAPPA $R = 5$ with a temporal resolution of 41 ms resulted in a reduction of 21 % and k-t GRAPPA $R = 8$ in a reduction of 71 % ($p < 0.001$).

3D visualization of arterial and portal venous hemodynamics

Both readers described complete visibility (= grade 2) for the majority of vascular segments in the hepatic arterial and portal venous systems with limitations for the small intrahepatic branches (Table 2). Flow visualization was limited for the right intrahepatic branch (in five of 80 scans for both readers A and B) and for the left intrahepatic branch (in 38 of 80 scans for reader A and in 39 of 80 scans for reader B) (Table 2). A significant difference was only seen between standard GRAPPA 2 and acceleration factor k-t GRAPPA 8 ($p = 0.028$) (Fig. 1).

3D flow visualization artifacts with leakage into adjacent vessels were observed for particle traces in 63 %

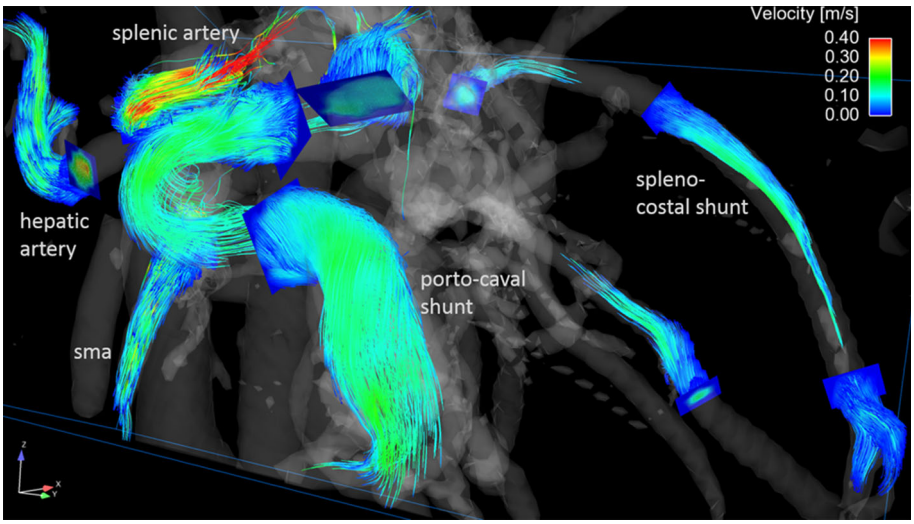

Fig. 2 3D particle traces visualization of the hepatic blood flow in a 30-year-old patient with advanced liver cirrhosis Child-Pugh class C for acceleration factor k-t GRAPPA $R = 5$. The liver hemodynamics of the patient present a large porto-caval shunt in the front and additional multiple spleno-costal shunts in the back

(reader A) and 59 % (reader B) of hepatic vessels (Table 2; Fig. 1). When comparing different acceleration factors, significant improvement was seen for visualization artifacts and noise between standard GRAPPA $R = 2$ and acceleration factor k-t GRAPPA $R = 3$ ($p < 0.001$). On the other hand, significantly more visualization artifacts and noise were observed between standard GRAPPA $R = 2$ and k-t GRAPPA $R = 8$ ($p < 0.001$) (Figs. 1, 2).

A Cohen's kappa of 0.92 represented excellent agreement between both readers for all visual assessment ratings.

Quantification of arterial and portal venous hemodynamics

Results for maximum and mean systolic velocities, net flow volume, and WSS are summarized in Table 3 and Fig. 3. Significantly lower values were observed for the maximum velocities between standard GRAPPA $R = 2$ and k-t GRAPPA $R = 3$ in the small intrahepatic branches (10 and 15 %) and hepatic and superior mesenteric arteries (13 and 14 %) ($p < 0.05$). k-t GRAPPA with $R = 8$ showed significantly reduced maximum velocity values compared to standard GRAPPA $R = 2$ for all arteries between 12 and 30 % ($p < 0.05$); Bland–Altman analysis demonstrated bias with a mean difference of 24 % (Fig. 3; Table 3).

There was less of an influence of k-t GRAPPA acceleration on net flow rate values with significant differences only occurring in the superior mesenteric vein for k-t GRAPPA $R = 3$ and in the portal vein for k-t GRAPPA $R = 5$ (temporal resolution 82 ms) revealing 22 and 14 % different flow rates, respectively, compared to standard GRAPPA $R = 2$ ($p < 0.05$).

WSS was significantly underestimated by 9–13 % for all vessels in the portal venous system for k-t GRAPPA $R = 5$ (temporal resolution 82 ms) compared to standard GRAPPA $R = 2$. In contrast, significantly higher values were observed for k-t GRAPPA $R = 5$ with higher temporal resolution (k-t GRAPPA 5 Tres41) in two veins (intrahepatic part of the main portal vein (8 %) and right intrahepatic portal vein branch (16 %) compared to standard GRAPPA $R = 2$ ($p < 0.05$). WSS was underestimated within the hepatic arterial system for k-t GRAPPA $R = 8$ compared to standard GRAPPA $R = 2$ (18–31 %, $p < 0.05$) with mean differences of 19 % in the Bland–Altman analysis (Fig. 3; Table 3).

Discussion

k-t-accelerated 4D flow MRI of the liver offered good image quality and low inter-observer variability. All k-t GRAPPA-accelerated 4D flow MRI acquisitions resulted in significant reductions in scan time. Although k-t GRAPPA $R = 8$ achieved the greatest acquisition time savings (71 %), noise and particle tracing artefacts, along with significantly lower values for peak velocities and WSS in the arterial system of the liver limit utility. 4D flow MRI using k-t acceleration factors $R = 3$ and $R = 5$ demonstrate good agreement with standard GRAPPA $R = 2$ for peak velocities and net flow rate quantification while realizing scan time savings of approximately 40 %. An improved temporal resolution for k-t GRAPPA $R = 5$ demonstrated good agreement at quantitative analysis with standard GRAPPA $R = 2$ with the exception of overestimating WSS in two vessel segments.

Acceleration with k-t GRAPPA was thoroughly investigated with respect to the reproducibility of flow and wall shear stress in a previously published study of the aorta [42]. Recent studies revealed good scan-rescan reproducibility and low inter- and intra-observer variability of flow quantification based on 4D flow MRI [15, 43]. Further studies investigating the use of PC MRI with parallel imaging techniques concluded that standard parallel imaging using GRAPPA with a reduction factor of $R = 2$ can be used as a reference standard as no significant underestimation of peak velocities was observed [27, 44].

Qualitative analyses with 3D streamlines and time-resolved 3D particle traces visualized all arterial and portal venous vessels of the liver except the small intrahepatic branches of the portal vein, most likely due to limitations of spatial resolution and the vessel size (1–2 mm of the intrahepatic branches vs. 10 mm in the main portal vein). For all acceleration factors, visualization artifacts with leakage of traces into adjacent vessels were identified in 63 % of acquisitions, which could be attributed to spatial blurring based on respiratory gating during the data acquisition with free breathing, and thus reduced effective spatial resolution in the z direction. Comparing different k-t GRAPPA acceleration factors, a significant improvement was seen for visualization artifacts and noise between standard acceleration factor GRAPPA 2 and k-t GRAPPA 3. This might be explained by better SNR performance of k-t GRAPPA reconstruction compared to standard GRAPPA for similar reduction factors due to the properties of uncorrelated noise of different time frames [31]. However, an undersampling of the 4D flow MRI data with acceleration factor of $R = 8$ resulted in significantly more visualization artifacts and noise. The scans in our study were obtained using a 12-element coil. Using coils with an increased number of receiver channels may improve the quality of 4D flow data with higher reduction factors.

Quantitative analysis demonstrated similar peak and mean velocity values for k-t GRAPPA acceleration factors $R = 3$ and $R = 5$ compared to the standard acceleration

Table 3 Bland–Altman analyses (mean bias ± 2SD) for arterial and portal venous flow parameters in the hepatic system illustrating the agreement between k-t GRAPPA 4D flow MRI acquisitions with acceleration factor of $R = 2$ versus $R = 3$, $R = 2$ versus $R = 5$, $R = 2$ versus $R = 5$ with temporal resolution 41 ms, and $R = 2$ versus $R = 8$

Bland–Altman analyses (difference in percentage normalized by the mean of the two compared)				
	GRAPPA 2 versus 3	GRAPPA 2 versus 5	GRAPPA 2 versus 5/41	GRAPPA 2 versus 8
Peak velocity (%)				
Superior mesenteric vein	1.1 ± 20.5	−6.6 ± 20.7	−8.0 ± 26.3	4.5 ± 22.5
Splenic vein	8.2 ± 23.0	8.2 ± 15.6	−1.6 ± 15.2	1.4 ± 21.1
Splenic–mesenteric confluence	3.8 ± 14.6	4.4 ± 11.3	−3.6 ± 14.9	4.9 ± 18.0
Intrahepatic portal vein	8.6 ± 19.6	−1.5 ± 14.9	−3.7 ± 10.9	5.4 ± 21.4
Right portal vein branch	14.4 ± 24.7*	6.8 ± 17.3	−6.9 ± 19.0	4.9 ± 27.9
Left portal vein branch	8.6 ± 11.8*	2.4 ± 13.9	−8.4 ± 10.4*	1.3 ± 25.2
Celiac trunk	2.4 ± 14.8	1.3 ± 17.1	0.8 ± 17.4	11.5 ± 18.4*
Splenic artery	−5.3 ± 16.4	−2.8 ± 13.8	−4.9 ± 13.4	20.9 ± 27.5*
Hepatic artery	12.8 ± 22.0*	7.4 ± 24.4	3.4 ± 19.3	22.7 ± 29.8*
Superior mesenteric artery	15.2 ± 19.5*	9.4 ± 21.0	4.0 ± 18.6	36.6 ± 22.8*
Mean velocity (%)				
Superior mesenteric vein	0.2 ± 14.7	−5.4 ± 18.2	−0.8 ± 18.6	−2.7 ± 16.4
Splenic vein	1.7 ± 14.9	0.6 ± 13.3	−0.9 ± 15.0	−4.2 ± 19.4
Splenic–mesenteric confluence	1.9 ± 13.2	0.5 ± 12.4	−2.6 ± 14.2	0.9 ± 16.8
Intrahepatic portal vein	5.0 ± 12.6	−2.1 ± 10.8	−2.9 ± 8.5	−0.3 ± 16.6
Right portal vein branch	5.0 ± 15.1	1.0 ± 15.5	−4.8 ± 12.9	−2.6 ± 22.4
Left portal vein branch	5.6 ± 12.0*	−0.8 ± 9.3	−4.6 ± 12.4	−2.7 ± 17.0
Celiac trunk	−1.6 ± 13.0	−4.3 ± 13.6	0.6 ± 14.0	−1.5 ± 15.7
Splenic artery	−4.8 ± 12.9	−6.1 ± 11.0*	−0.6 ± 11.1	2.4 ± 19.9
Hepatic artery	1.6 ± 20.7	−6.2 ± 19.2	0.7 ± 14.1	−3.8 ± 18.7
Superior mesenteric artery	−3.3 ± 15.6	−4.8 ± 15.3	2.4 ± 16.1	−0.6 ± 17.4
Flow volume (%)				
Superior mesenteric vein	−20.7 ± 25.1*	−12.8 ± 42.2	0.7 ± 31.0	−10.6 ± 33.6
Splenic vein	4.0 ± 19.8	5.5 ± 27.3	5.4 ± 30.5	0.1 ± 29.3
Splenic–mesenteric confluence	−7.9 ± 19.0	−15.4 ± 19.2*	−0.7 ± 21.5	−12.5 ± 27.5
Intrahepatic portal vein	−4.9 ± 20.2	−15.0 ± 24.5*	−1.3 ± 21.7	−4.9 ± 24.8
Right portal vein branch	−11.5 ± 46.1	−14.1 ± 35.7	3.0 ± 30.6	−6.9 ± 48.9
Left portal vein branch	4.1 ± 35.7	−9.7 ± 21.7	2.2 ± 28.7	−5.4 ± 31.5
Celiac trunk	−13.1 ± 23.3	−8.9 ± 25.3	1.7 ± 20.1	−12.3 ± 32.2
Splenic artery	−5.1 ± 13.2	−3.5 ± 13.7	9.7 ± 16.2*	9.2 ± 22.3
Hepatic artery	−2.0 ± 37.2	−11.1 ± 36.5	3.0 ± 24.5	−7.6 ± 44.4
Superior mesenteric artery	2.2 ± 21.4	−5.5 ± 25.9	−0.2 ± 16.9	−2.2 ± 25.9
WSS (%)				
Superior mesenteric vein	17.3 ± 18.0*	13.3 ± 22.9*	6.2 ± 27.8	10.4 ± 31.1
Splenic vein	8.9 ± 23.0	11.4 ± 16.0*	−5.1 ± 18.7	−1.9 ± 18.5
Splenic-mesenteric confluence	9.5 ± 14.7*	16.1 ± 13.3*	0.3 ± 19.4	10.8 ± 27.3
Intrahepatic portal vein	10.6 ± 16.3*	9.4 ± 16.4*	−7.6 ± 13.3*	4.8 ± 24.4
Right portal vein branch	14.4 ± 26.0	12.1 ± 14.2*	−15.5 ± 13.0*	−3.4 ± 28.4
Left portal vein branch	11.0 ± 14.7*	15.9 ± 19.1*	0.0 ± 20.8	5.4 ± 26.9
Celiac trunk	3.8 ± 19.6	3.7 ± 18.5	−7.0 ± 26.6	17.5 ± 25.1*
Splenic artery	−4.2 ± 20.4	−2.9 ± 15.0	−8.4 ± 14.3*	18.3 ± 25.2*
Hepatic artery	8.3 ± 21.3	15.0 ± 18.9*	6.6 ± 18.7	24.2 ± 25.0*
Superior mesenteric artery	9.2 ± 27.2	5.5 ± 15.1	1.5 ± 22.5	26.7 ± 28.2*

* Significant difference to standard acceleration factor GRAPPA $R = 2$ ($p < 0.05$)

$R = 2$. However, quantitation was limited for the small intrahepatic branches and the hepatic and superior mesenteric arteries due to the small vessel size. Flow volume values were comparable between standard GRAPPA $R = 2$ and k-t GRAPPA $R = 3$ and $R = 5$ with few limitations in the portal venous system (superior mesenteric vein for k-t GRAPPA $R = 3$ and portal vein for k-t GRAPPA $R = 5$ temporal resolution 82 ms). When comparing the quantitative results to previous studies at 3T with similar 4D flow MRI protocols using standard GRAPPA $R = 2$ [43], the differences between the acceleration factors were larger than the variations attributed to scan-rescan analyses. For example, Stankovic et al. [43] performed scan-rescan analyses and demonstrated average differences for the maximum velocities of 2 % for the portal venous system and 3 % for the arterial system. In our study, significantly lower values were obtained of up to 15 % for the maximum velocities between standard GRAPPA $R = 2$ and k-t GRAPPA $R = 3$ in the small intrahepatic branches and hepatic and superior mesenteric arteries ($p < 0.05$). A k-t GRAPPA acceleration factor of $R = 8$ revealed significantly reduced maximum velocity values compared to standard GRAPPA $R = 2$ for all arteries of up to 30 % ($p < 0.05$).

When comparing mean flow volume values, scan-rescan analysis on a prior study demonstrated average differences of 6 % for the portal venous system [43]. Our results yielded only a few significantly higher differences on net flow rate values only occurring in the superior mesenteric vein for k-t GRAPPA $R = 3$ and in the portal vein for k-t GRAPPA $R = 5$ revealing 22 and 14 % higher flow rates, respectively, ($p < 0.05$). Hence, differences in maximum velocity and net flow cannot be attributed to differences in patient physiology or scan-rescan differences alone and is, therefore, a result of the differences in acceleration technique between acquisitions.

Calculations of WSS demonstrated similar results in the arterial system while the portal venous system offered significant differences for almost all vessels. Though using a proper registration for the segmentation the vessel lumen delineation was limited due to spatial resolution, especially in the portal venous system. We hypothesize that the results for WSS might be confounded due to differences in the requisite manual vessel segmentation in the portal venous system, and hence the delineation of the vessel walls resulting in errors in WSS analysis.

Despite shorter scan times for accelerated measurements, the spatial resolution was kept constant across acquisitions in order to maintain the SNR. Therefore, only the temporal resolution (in one additional scan $R = 5$) was increased to investigate the impact in terms of temporal filtering. A clear temporal low-pass filter effect for $R = 8$ could be observed resulting in significantly reduced peak velocities (see Fig. 3). The higher temporal resolution revealed a trend to higher peak velocities (only significant in the left portal vein branch), suggesting a low pass filtering effect at a temporal resolution of 82 ms. On the other hand, differences in net flow volumes were greater compared to peak velocities or mean velocities (Fig. 3), suggesting that differences in the segmented vessel area had a higher impact on the flow volume compared to filter effects caused by k-t acceleration (except for $R = 8$) (Fig. 3).

Concerning the scan time, only minor improvements were seen of approximately 27 %, most probably due to the predefined scan protocol and the variable navigator efficiencies for the different acceleration factors. The most undersampled acquisition with k-t GRAPPA acceleration $R = 8$ revealed significantly different results for quantification of both hepatic arterial peak velocities and WSS.

Our results are similar to the experience of other investigators [31, 44, 45]. Baltes et al. [45] applied k-t SENSE and k-t BLAST with an acceleration of $R = 5$ and 8 for 2D-PC MRI in the ascending aorta. Their results demonstrated good agreement of flow parameters for $R = 5$ and a slight temporal low-pass filtering for $R = 8$. Former studies with identical k-t GRAPPA-accelerated reconstruction of 4D flow MRI measurements in the thoracic aorta suggested the possibility to use even higher acceleration factors of up to $R = 8$ [31]. However, these studies were based on retrospectively undersampled data, whereas the present study relies on the acquisition of truly undersampled data. A recent study for assessment of the thoracic aorta using the k-t GRAPPA reconstruction algorithm with different receiver coils showed significantly reduced scan times for $R = 3$, $R = 5$, and $R = 8$, respectively, while the image quality was maintained. The authors concluded that k-t GRAPPA with accelerations of $R = 3$ or $R = 5$ could compete with a standard GRAPPA $R = 2$ [46]. In comparison to imaging the thoracic aorta, imaging of liver hemodynamics is more challenging necessitating evaluation of higher flow in the arterial branches, but a lower flow in the portal venous system. Based on a different region of interest and different velocity hemodynamics our study showed similar quantification results for velocities and net flow for k-t GRAPPA with acceleration of $R = 3$ or $R = 5$ compared to standard GRAPPA $R = 2$.

This study has several limitations. The study cohort entirely comprises healthy volunteers, limiting generalizability of our results to patients with liver disease. Similarly, the generalizability of image quality and visualization is limited as ascites and other sequellae of chronic liver disease may reduce the image quality. Another limitation is the lack of a gold standard to compare the hemodynamic data. Because of limited inter-observer

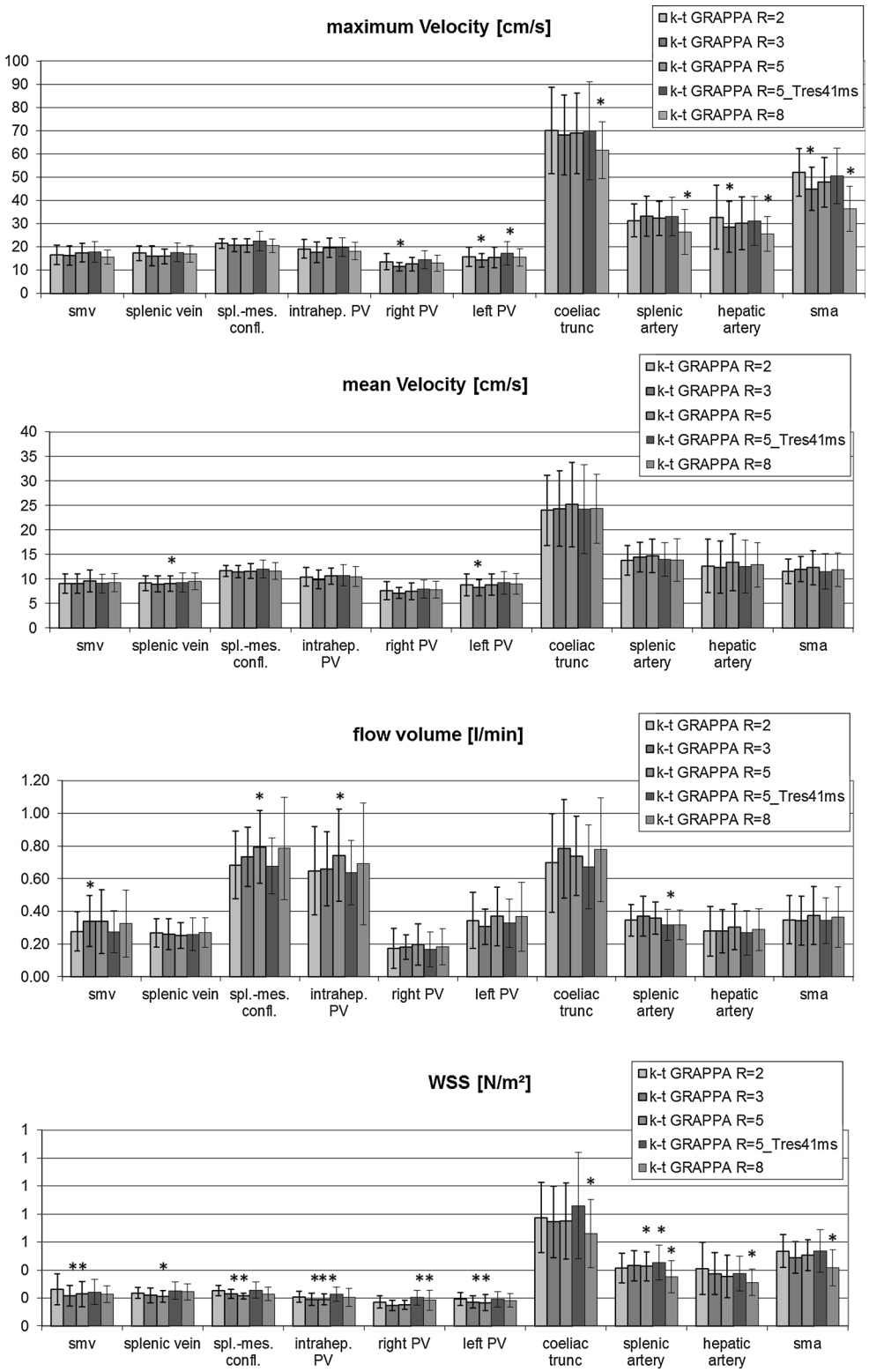

Fig. 3 Flow quantification for all controls using 4D flow MRI with standard GRAPPA $R = 2$ and acceleration factor k-t GRAPPA $R = 3$, $R = 5$, $R = 5$ Tres 41, and $R = 8$. Each bar represents the standard deviation over 16 volunteers. (*Significant difference compared to standard GRAPPA $R = 2$, $p < 0.05$) (smv = superior mesenteric vein, spl.-mes. confl. = splenic–mesenteric confluence, intrahep. PV = intrahepatic portal vein, PV = portal vein, sma = superior mesenteric artery)

reproducibility of the Doppler US measurements mentioned in the literature, and difficulties with correct plane positioning for 2D PC MRI in the complex liver vasculature, none of these methods were considered for comparison. Finally, a further limitation of the study is the non-randomized scan order with a predefined succession of 4D flow MRI scans with different acceleration factors. This may have resulted in different navigator efficiencies for different acceleration factors, influencing our assessment of acquisition times.

Conclusion

In conclusion k-t GRAPPA-accelerated assessment of liver hemodynamics using 4D flow MRI is feasible for acceleration factors $R = 3$ and $R = 5$ while achieving a significant reduction in scan time. k-t GRAPPA acceleration with factors $R = 3$ and $R = 5$ showed similar results compared to the standard GRAPPA $R = 2$ for peak velocity and net flow rate evaluation, but were limited for WSS evaluation in the portal venous system. Hence, our results in volunteers suggest that the optimal balance between acquisition time, visualization, and quantification at 4D flow MRI k-t GRAPPA $R = 3$ and $R = 5$ should be further validated in the clinic compared to standard GRAPPA $R = 2$. k-t GRAPPA acceleration factor $R = 8$ is not feasible for the liver hemodynamic assessment due to higher noise and temporal filtering as indicated by the quantitative results. Future studies are necessary to validate k–t-accelerated 4D flow MRI for the evaluation of liver hemodynamics and realize scan time savings in patients with liver disease.

Acknowledgments Supported by the German Research Foundation (DFG) under Award Number STA 1288/2-1 and JU 2687/4-1.

Conflict of interest The authors declare that they have no conflict of interest.

Ethical standard The study has been approved by our local ethics committee and has therefore been performed in accordance with the ethical standards laid down in the 1964 Declaration of Helsinki and its later amendments. All persons gave their informed consent prior to their inclusion in the study. Details that might disclose the identity of the subjects under study were omitted.

References

1. Bell BP, Manos MM, Zaman A, Terrault N, Thomas A, Navarro VJ, Dhotre KB, Murphy RC, Van Ness GR, Stabach N, Robert ME, Bower WA, Bialek SR, Sofair AN (2008) The epidemiology of newly diagnosed chronic liver disease in gastroenterology practices in the United States: results from population-based surveillance. Am J Gastroenterol 103(11):2727–2736; quiz 2737
2. Groszmann RJ (1994) Hyperdynamic circulation of liver disease 40 years later: pathophysiology and clinical consequences. Hepatology 20(5):1359–1363
3. Berzigotti A, Seijo S, Reverter E, Bosch J (2013) Assessing portal hypertension in liver diseases. Expert Rev Gastroenterol Hepatol 7(2):141–155
4. Bintintan A, Chira RI, Mircea PA (2013) Non-invasive ultrasound-based diagnosis and staging of esophageal varices in liver cirrhosis. A systematic review of the literature published in the third millenium. Med Ultrason 15(2):116–124
5. Malek AM, Jackman R, Rosenberg RD, Izumo S (1994) Endothelial expression of thrombomodulin is reversibly regulated by fluid shear stress. Circ Res 74(5):852–860
6. Lehoux S, Tedgui A (2003) Cellular mechanics and gene expression in blood vessels. J Biomech 36(5):631–643
7. Truong U, Fonseca B, Dunning J, Burgett S, Lanning C, Ivy DD, Shandas R, Hunter K, Barker AJ (2013) Wall shear stress measured by phase contrast cardiovascular magnetic resonance in children and adolescents with pulmonary arterial hypertension. J Cardiovasc Magn Reson 15:81
8. Lorenz R, Bock J, Barker AJ, von Knobelsdorff-Brenkenhoff F, Wallis W, Korvink JG, Bissell MM, Schulz-Menger J, Markl M (2014) 4D flow magnetic resonance imaging in bicuspid aortic valve disease demonstrates altered distribution of aortic blood flow helicity. Magn Reson Med 71(4):1542–1553
9. Markl M, Frydrychowicz A, Kozerke S, Hope M, Wieben O (2012) 4D flow MRI. J Magn Reson Imaging 36(5):1015–1036
10. Stankovic Z, Allen BD, Garcia J, Jarvis KB, Markl M (2014) 4D flow imaging with MRI. Cardiovasc Diagn Ther 4(2):173–192
11. Wentland AL, Grist TM, Wieben O (2013) Repeatability and internal consistency of abdominal 2D and 4D phase contrast MR flow measurements. Acad Radiol 20(6):699–704
12. Stankovic Z, Frydrychowicz A, Csatari Z, Panther E, Deibert P, Euringer W, Kreisel W, Russe M, Bauer S, Langer M, Markl M (2010) MR-based visualization and quantification of three-dimensional flow characteristics in the portal venous system. J Magn Reson Imaging 32(2):466–475
13. Frydrychowicz A, Landgraf BR, Niespodzany E, Verma RW, Roldan-Alzate A, Johnson KM, Wieben O, Reeder SB (2011) Four-dimensional velocity mapping of the hepatic and splanchnic vasculature with radial sampling at 3 tesla: a feasibility study in portal hypertension. J Magn Reson Imaging 34(3):577–584
14. Stankovic Z, Csatari Z, Deibert P, Euringer W, Blanke P, Kreisel W, Abdullah Zadeh Z, Kallfass F, Langer M, Markl M (2012) Normal and altered three-dimensional portal venous hemodynamics in patients with liver cirrhosis. Radiology 262(3):862–873
15. Roldan-Alzate A, Frydrychowicz A, Niespodzany E, Landgraf BR, Johnson KM, Wieben O, Reeder SB (2013) In vivo validation of 4D flow MRI for assessing the hemodynamics of portal hypertension. J Magn Reson Imaging 37(5):1100–1108
16. Stankovic Z, Csatari Z, Deibert P, Euringer W, Jung B, Kreisel W, Geiger J, Russe MF, Langer M, Markl M (2013) A feasibility study to evaluate splanchnic arterial and venous hemodynamics by flow-sensitive 4D MRI compared with Doppler ultrasound in patients with cirrhosis and controls. Eur J Gastroenterol Hepatol 25(6):669–675
17. Taouli B (2012) Diffusion-weighted MR imaging for liver lesion characterization: a critical look. Radiology 262(2):378–380
18. Brodsky EK, Bultman EM, Johnson KM, Horng DE, Schelman WR, Block WF, Reeder SB (2013) High-spatial and high-temporal resolution dynamic contrast-enhanced perfusion imaging of the liver with time-resolved three-dimensional radial MRI. Magn Reson Med. doi:10.1002/mrm.24727
19. Muthupillai R, Lomas DJ, Rossman PJ, Greenleaf JF, Manduca A, Ehman RL (1995) Magnetic resonance elastography by direct visualization of propagating acoustic strain waves. Science 269(5232):1854–1857
20. Stankovic Z, Blanke P, Markl M (2012) Usefulness of 4D MRI flow imaging to control TIPS function. Am J Gastroenterol 107(2):327–328
21. Kato S, Kitagawa K, Ishida N, Ishida M, Nagata M, Ichikawa Y, Katahira K, Matsumoto Y, Seo K, Ochiai R, Kobayashi Y, Sakuma H (2010) Assessment of coronary artery disease using magnetic resonance coronary angiography: a national multicenter trial. J Am Coll Cardiol 56(12):983–991
22. Piccini D, Monney P, Sierro C, Coppo S, Bonanno G, van Heeswijk RB, Chaptinel J, Vincenti G, de Blois J, Koestner SC, Rutz T, Littmann A, Zenge MO, Schwitter J, Stuber M (2014) Respiratory self-navigated postcontrast whole-heart coronary MR angiography: initial experience in patients. Radiology 270(2):378–386

23. Johnson KM, Lum DP, Turski PA, Block WF, Mistretta CA, Wieben O (2008) Improved 3D phase contrast MRI with off-resonance corrected dual echo VIPR. Magn Reson Med 60(6):1329–1336
24. Markl M, Harloff A, Bley TA, Zaitsev M, Jung B, Weigang E, Langer M, Hennig J, Frydrychowicz A (2007) Time-resolved 3D MR velocity mapping at 3T: improved navigator-gated assessment of vascular anatomy and blood flow. J Magn Reson Imaging 25(4):824–831
25. Griswold MA, Jakob PM, Heidemann RM, Nittka M, Jellus V, Wang J, Kiefer B, Haase A (2002) Generalized autocalibrating partially parallel acquisitions (GRAPPA). Magn Reson Med 47(6):1202–1210
26. Pruessmann KP, Weiger M, Scheidegger MB, Boesiger P (1999) SENSE: sensitivity encoding for fast MRI. Magn Reson Med 42(5):952–962
27. Thunberg P, Karlsson M, Wigstrom L (2003) Accuracy and reproducibility in phase contrast imaging using SENSE. Magn Reson Med 50(5):1061–1068
28. Pedersen H, Kozerke S, Ringgaard S, Nehrke K, Kim WY (2009) k-t PCA: temporally constrained k-t BLAST reconstruction using principal component analysis. Magn Reson Med 62(3):706–716
29. Huang F, Akao J, Vijayakumar S, Duensing GR, Limkeman M (2005) k-t GRAPPA: a k-space implementation for dynamic MRI with high reduction factor. Magn Reson Med 54(5):1172–1184
30. Tsao J, Boesiger P, Pruessmann KP (2003) k-t BLAST and k-t SENSE: dynamic MRI with high frame rate exploiting spatio-temporal correlations. Magn Reson Med 50(5):1031–1042
31. Jung B, Stalder AF, Bauer S, Markl M (2011) On the under-sampling strategies to accelerate time-resolved 3D imaging using k-t-GRAPPA. Magn Reson Med 66(4):966–975
32. Jung B, Honal M, Ullmann P, Hennig J, Markl M (2008) Highly k-t-space-accelerated phase-contrast MRI. Magn Reson Med 60(5):1169–1177
33. Bernstein MA, Zhou XJ, Polzin JA, King KF, Ganin A, Pelc NJ, Glover GH (1998) Concomitant gradient terms in phase contrast MR: analysis and correction. Magn Reson Med 39(2):300–308
34. Bock J, Kreher BW, Hennig J, Markl M (2007) Optimized pre-processing of time-resolved 2D and 3D Phase Contrast MRI data. In: Proceedings of the 15th scientific meeting, international society for magnetic resonance in medicine. Berlin, Abstract 3138
35. Walker PG, Cranney GB, Scheidegger MB, Waseleski G, Pohost GM, Yoganathan AP (1993) Semiautomated method for noise reduction and background phase error correction in MR phase velocity data. J Magn Reson Imaging 3(3):521–530
36. Bock J, Frydrychowicz A, Stalder AF, Bley TA, Burkhardt H, Hennig J, Markl M (2010) 4D phase contrast MRI at 3 T: effect of standard and blood-pool contrast agents on SNR, PC-MRA, and blood flow visualization. Magn Reson Med 63(2):330–338
37. Buonocore MH (1998) Visualizing blood flow patterns using streamlines, arrows, and particle paths. Magn Reson Med 40(2):210–226
38. Likert R (1932) A technique for the measurement of attitudes. Arch Psychol 140:1–55
39. Stalder AF, Russe MF, Frydrychowicz A, Bock J, Hennig J, Markl M (2008) Quantitative 2D and 3D phase contrast MRI: optimized analysis of blood flow and vessel wall parameters. Magn Reson Med 60(5):1218–1231
40. Landis JR, Koch GG (1977) The measurement of observer agreement for categorical data. Biometrics 33(1):159–174
41. Bland JM, Altman DG (1986) Statistical methods for assessing agreement between two methods of clinical measurement. Lancet 1(8476):307–310
42. Markl M, Wallis W, Harloff A (2011) Reproducibility of flow and wall shear stress analysis using flow-sensitive four-dimensional MRI. J Magn Reson Imaging 33(4):988–994
43. Stankovic Z, Jung B, Collins J, Russe MF, Carr J, Euringer W, Stehlin L, Csatari Z, Strohm PC, Langer M, Markl M (2013) Reproducibility study of four-dimensional flow MRI of arterial and portal venous liver hemodynamics: influence of spatio-temporal resolution. Magn Reson Med. doi:10.1002/mrm.24939
44. Stadlbauer A, van der Riet W, Globits S, Crelier G, Salomonowitz E (2009) Accelerated phase-contrast MR imaging: comparison of k-t BLAST with SENSE and Doppler ultrasound for velocity and flow measurements in the aorta. J Magn Reson Imaging 29(4):817–824
45. Baltes C, Kozerke S, Hansen MS, Pruessmann KP, Tsao J, Boesiger P (2005) Accelerating cine phase-contrast flow measurements using k-t BLAST and k-t SENSE. Magn Reson Med 54(6):1430–1438
46. Schnell S, Markl M, Entezari P, Mahadewia RJ, Semaan E, Stankovic Z, Collins J, Carr J, Jung B (2013) k-t GRAPPA accelerated four-dimensional flow MRI in the aorta: effect on scan time, image quality, and quantification of flow and wall shear stress. Magn Reson Med. doi:10.1002/mrm.24925